3 Biotech (2021) 11:342
https://doi.org/10.1007/s13205-021-02888-4

ORIGINAL ARTICLE

Application of mycogenic silver/silver oxide nanoparticles in electrochemical glucose sensing; alongside their catalytic and antimicrobial activity

Sk Najrul Islam[1] · Syed Mohd Adnan Naqvi[1] · Sadia Parveen[1] · Absar Ahmad[1]

Received: 12 March 2021 / Accepted: 7 June 2021 / Published online: 17 June 2021

Abstract

The present work describes the biofabrication of highly stable, water-dispersible mycogenic silver/silver (I) oxide nanoparticles (Ag/Ag_2O NPs) alongside its potential applications in non-enzymatic electrochemical glucose sensing and catalytic degradation of methylene blue (MB) dye in presence of reducing agent $NaBH_4$. These Ag/Ag_2O NPs were fabricated from silver oxide micro powder using endophytic fungus *Fusarium oxysporum* based environmentally friendly, bio-inspired, top-down approach which is highly reproducible, reliable, and cheap. Bacterial and plant-mediated bottom-up approaches have been previously reported for the production of Ag/Ag_2O NPs. Bacterial methods are not economical as they require expensive sophisticated instruments for separation and purification. Similarly, plant-based means of synthesis are not reliable and reproducible due to geographical and seasonal variability's. UV–Visible spectroscopy, TEM, SAED, FTIR, XRD, TGA, and DSC were used for the characterization and investigation of thermal properties of mycogenic nanoparticles and their antimicrobial activity was evaluated by filter- paper bioassay technique.

Keywords Antimicrobial · Catalyst · Electrochemical sensing · Nanoparticles · Silver/silver oxide

Introduction

Nanotechnology is the branch of engineering that involves the study of materials having one or more dimensions of the size of 1–100 nm. In recent decades, nanotechnology has flourished due to their size-dependent novel properties and its wide applications in technology (Sharma et al. 2009) Among different types of inorganic nanomaterial, nano-sized metal oxide especially Silver Oxide nanoparticles have achieved considerable importance for their potential application in different branches of science and technology as well as medical science. Ag_2O was used as a catalyst (Derikvand et al. 2010; Wang et al. 2011) for the oxidation of organic molecules and oxygen evolution by water splitting. The material is also reported for its application in fuel cells (Pishbin et al. 2007), sensors (Petrov et al. 2008), photovoltaic cells (Ida et al. 2008), and biomedicine (Tarahovsky et al. 2008). Various methods including the chemical method (Yong et al. 2013), electrochemical method (Wei et al. 2011) have been reported for the fabrication of silver oxide nanoparticles. However, most of the techniques required high temperatures, toxic chemicals, while also being capital intensive. Thus, it is the prime requirement to develop non-polluting, eco-friendly nano synthesis protocols that can generate safe, stable, reliable nanomaterials. The biological 'green' nanofabrication routes which have recently been developed are in complete synchronization with the environment. Our group is amongst the key contributors (Islam et al. 2021; Shankar et al. 2004; Bansal et al. 2006; Ahmad et al. 2007; Khan et al. 2014) to the field. Recently biosynthesis of silver oxide nanoparticles has been reported using plant extract (Manikandan et al. 2017; Jalees et al. 2018) and bacteria (Dhoondia et al. 2012). In the present work, we have biotransformed Ag_2O micro powder into Ag/Ag_2O NPs using endophytic fungus *Fusarium oxysporum* followed by the investigation of electrochemical, thermal, catalytic, and antimicrobial activity. To the best of our knowledge, it's the first report of mycogenic fabrication of Ag/Ag_2O NPs using

✉ Absar Ahmad
aahmad786in@gmail.com; director.inc@amu.ac.in

[1] Interdisciplinary Nanotechnology Centre (INC), Z. H. College of Engineering and Technology, Aligarh Muslim University, AMU, Aligarh, UP 202002, India

fungal biomass. Fungus-based synthesis of nanomaterials is more advantageous as compared with other biological methods because fungal biomass is easily separable from nanoparticle solution by simple filtration method, easily isolatable by plating, the potential for large-scale production, abundant in nature, and easy to handling (Khan et al. 2017). Non-enzymatic glucose sensing was carried out electrochemically because in medical science diabetes becomes a serious health problem and thus glucose level in blood should be investigated. Different enzymatic and non-enzymatic sensing methods (Fuglerud et al. 2019; Lee et al. 2018) have been reported. In the enzyme base sensor, there are some drawbacks i.e., low chemical and thermal stability, poor reproducibility, and expensive costs. Thus researchers are attracted to enzyme-free electrochemical determination using a nanomaterial modified electrode (Shahriary et al. 2015; Chen et al. 2012). Different metal, metal oxide and their nanocomposite-based modified electrode were used for enzyme-free electrochemical glucose sensing (Maurício et al. 2017; Shabbir et al 2019; Zhu et al. 2016). Here mycogenic silver oxide nanoparticles were used as modified electrodes to detect glucose through the enzyme-free electrochemical method.

In this developing world, one of the major threats to human health and aquatic life is organic dye molecules which are extensively used in different industries like textiles, paints, paper, cosmetics, plastics, etc. Among various hazardous organic dyes thiazine dye Methylene Blue (MB), also known as methylthioninium chloride, is mainly utilized in biomedical, biological, and biochemical fields. The excessive use of this MB dye causes environmental pollution and toxicity. Thus removal of this dye from water is of prime importance for human beings and aquatic life as well. Nanocatalyst-based degradation of MB achieved a prominent place as nanoparticles provide a large surface-to-volume ratio, high shelf life and enhanced catalytic activity. Silver nanoparticles-based catalytic degradation of MB in presence of $NaBH_4$ has been investigated (Edison et al. 2016; Saha et al. 2017). Herein, we have investigated the catalytic activity of mycogenic Ag/Ag_2O NPs on the degradation of MB in the presence of reducing agent $NaBH_4$. Along with this thermal and antimicrobial activity of Ag/Ag_2O NPs were also investigated as silver shows antimicrobial activity (Ibarra et al. 2018).

Experimental section

Chemicals

AR grade Silver (I) Oxide micropowder was purchased from SRL, agarose from CDH whereas KOH, acetone, and D-glucose with AR grade was obtained from Qualigens. Apart from this Malt extract, Yeast extract, and Peptone from Hi-media were used without further purification.

Isolation, purification and maintenance of endophytic fungus *Fusarium oxysporum*

The endophytic fungus, *Fusarium oxysporum* was isolated from the plant parts such as leaves and maintained on potato dextrose agar (PDA) slants at 25 °C. The stoke cultures were maintained by subculturing at monthly intervals. After growing the fungus at pH 7 and 25 °C for 96 h, the PDA slants were preserved at 15 °C. From an actively growing stoke culture, subcultures were made on a fresh slant and after 96 h of incubation at pH 7 and 25 °C, were used as the starting material for fermentation and biotransformation experiments. For the biotransformation of micron size Ag_2O into Ag/Ag_2O nanoparticles, the fungus was grown in 500 ml Erlenmeyer flask containing 100 ml of MGYP medium which is composed of malt extract (0.3%), glucose (1%), yeast extract (0.3%), peptone (0.1%). The culture was grown with continuous shaking on a rotary shaker (200 rpm) at 25 °C for 96 h. After 96 h of fermentation, mycelial mass was separated from the culture broth by centrifugation (7000 rpm) at 15 °C for 20 min and then mycelia was washed thrice with sterile distilled water under sterile condition.

Biotransformation of Ag_2O micro powder into Ag/Ag_2O nanoparticles

The harvested mycelia mass (30 g) was then resuspended in 100 ml 0.1% Ag_2O micro powder in 500 ml Erlenmeyer flask at pH 7 at 25 °C and maintained under shaking conditions at 200 rpm. The reaction mixture was monitored for biotransformation for change in colour black to brown. The fungal mycelia were separated from the respective reaction mixture by filtration using Whatman filter paper. The filtrate containing nanoparticles were lyophilized to powder form for easy handling and further characterization.

Characterization techniques of mycogenic Ag/Ag_2O nanoparticles

The Cary 5000 UV–Vis–NIR spectrophotometer was used for recording UV- Visible spectra of mycogenic Ag/Ag_2O NPs at wavelengths from 200 to 800 nm to obtain initial conformation of Ag/Ag_2O NPs production. Fourier transform infrared (FTIR) spectra were recorded at wavenumber ranges from 400 to 4000 cm^{-1} for examining the functional biomolecules coated on silver oxide nanoparticles.

Whereas the X-ray powder diffraction (XRD) technique was executed to obtain the crystalline phase and unit cell dimensions using a Rigaku X-ray diffractometer. Most importantly, Ag/Ag_2O NPs were characterized by Transmission Electron Microscopy (TEM, JEM-JEOL, JAPAN), High-resolution transmission electron microscopy (HR-TEM), and selected area electron diffraction (SAED) pattern for investigation of the particles size, shape, crystalline structure, and surface morphology of biotransformed Ag/Ag_2O NPs.

Electrochemical measurement

The electrochemical activity of micron Ag_2O particles and mycogenic Ag/Ag_2O nanoparticles has been studied by performing Cyclic Voltammetry (CV) in a three-electrode cell. In the electrochemical study, modified microelectrodes with silver oxide and Ag/Ag_2O nanoparticles were separately used as a working electrode whereas the remaining two were platinum countered electrode and Ag/AgCl reference electrode. The individual working electrodes were made by using a drop-casting technique in which 50 µl of each aqueous solution (micron Ag_2O and Ag/Ag_2O nanoparticles) having a concentration of 1 mM were suspended on Glassy carbon electrode (GCE) with subsequent evaporation of H_2O molecules. We also used 1 M KOH solution as an electrolyte for performing CV at room temperature. The recording of voltammograms was started from 0 V in the positive direction with a sweep rate of 50 mVs^{-1} in the potential range −1.0 V to + 1.0 V.

Non-enzymatic glucose sensing

Enzyme-free glucose sensing was carried out by recording a cyclic voltammogram of 1 M KOH solution in the absence/presence of glucose. The five different concentrations (25, 50, 75, 100, and 125 µmol/L) of glucose were used to investigate the variation of the current peak. To obtain magnified peaks, the scanning was performed in a potential window ranges from 0 V to 1.0 V with the same scan rate of 50 mVs − 1 and the same starting potential 0 V in the positive direction. The working electrodes were constructed by dropping 50 µl of 1 mM micron Ag_2O solution and mycogenic Ag_2O nanoparticles solution onto GCE surface.

Catalytic degradation of MB dye

Time and NPs weight-dependent catalytic activity of mycogenic Ag/Ag_2O NPs was investigated on the degradation of MB dye in the presence of reducing agent $NaBH_4$. For time-dependent experiment, 2 ml of aqueous $NaBH_4$ solution (50 mM) and 1 ml of Ag/Ag_2O NPs solution (0.1 mg/ml) were added to 2 ml of aqueous MB solution (0.1 mM) and UV–Vis spectra of the solution mixture were recorded at a regular time interval of 10 min using UV–Vis–NIR spectrophotometer. Similarly, NPs weight-dependent dye degradation activity was investigated by recording UV–Vis absorption maxima of the aliquots with different dosages of Ag/Ag_2O NPs from 0.1 mg/ml to 0.5 mg/ml at a fixed time of 10 min. For the control, the same experiment was carried out with 0.5 mg/ml of Ag_2O micropowder.

Thermal analysis

Simultaneous thermogravimetric analysis and Differential scanning calorimetry (TGA/DSC) techniques were used to observe the behavior of Ag/Ag_2O NPs at different temperatures and the study of thermal properties (decomposition, enthalpy of reaction, and thermal stability) of biotransformed silver/silver oxide nanoparticles. For TGA analysis alumina was used as reference material.

Antimicrobial activity (filter paper bioassay) of mycogenic Ag/Ag_2O NPs

The fungus *Aspergillus niger* and Gram-positive bacterium *Bacillus subtilis* were maintained on potato dextrose agar (PDA) and nutrient agar (NA) slant respectively. Stoke cultures were maintained by subculturing at monthly intervals. From an actively growing stoke culture, subcultures were made on fresh slants and after 96 h of incubation at pH 7 and 25 °C, were used as the starting material for antimicrobial activity.

Freshly prepared spore suspension of test cultures was immediately overlaid on the surface of sterile PD agar (*Aspergillus niger*) and nutrient agar (*Bacillus subtilis*) plates (100 mm diameter). These plates were incubated at 25–28 °C for few hours for initial germination and facilitation of vegetative growth. Sterile filter paper (Whatman no 3, 1 square centimeter in size) was placed at three places and named a, b, c. Soon after, 100 µl of mycogenic Ag/Ag_2O NPs solution was loaded on filter paper b (50 µg/100 µl) and c (100 µg/100 µl). For negative control, only water was loaded on the filter paper a. The antibacterial and antifungal activities were evaluated after 24 h and 72 h respectively by examining the zone of inhibition across the filter paper.

Results and discussion

The present endophytic fungus was isolated in the laboratory and identified as *Fusarium oxysporum* based on cultural and morphological characteristics. The fungus when reacted

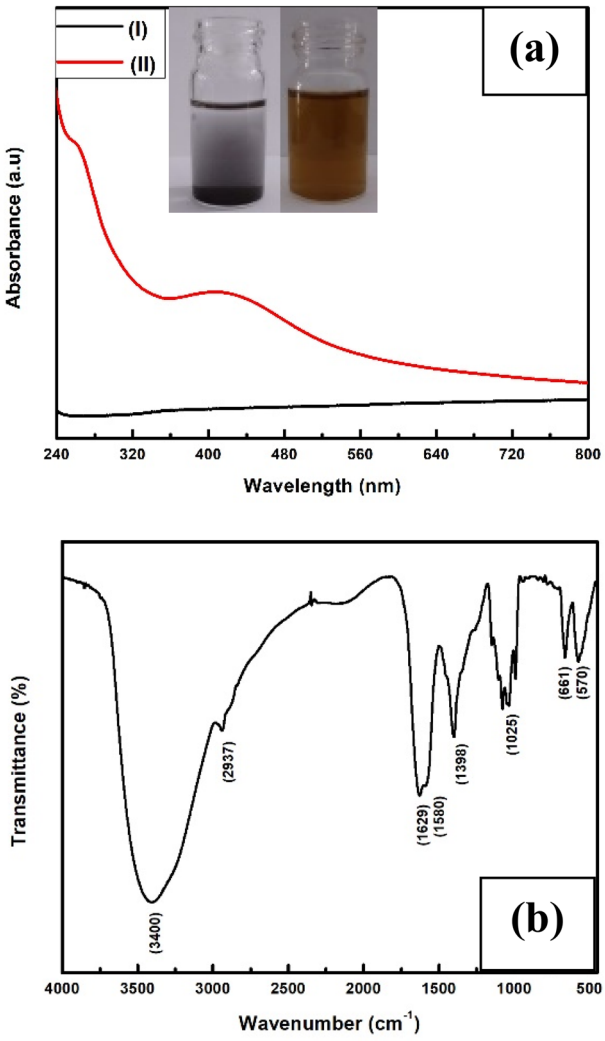

Fig. 1 **a** UV–Visible spectrum of (I) untreated Ag_2O micropowder and (II) biotransformed Ag/Ag_2O nanoparticles. The inset shows a glass vial containing untreated Ag_2O solution before (glass vial on the left side) and after reaction with fungal biomass (glass vial on the right side). **b** FT-IR spectra of biotransformed silver/silver oxide nanoparticles

with 0.1% Ag_2O (aqueous solution) at room temperature for 72 h on a rotary shaker (200 rpm), resulted in the extracellular synthesis of Ag/Ag_2O NPs and characterized by various standard techniques. UV–Vis spectroscopic measurement was carried out for the preliminary characterization of biotransformed Ag/Ag_2O NPs. Figure 1a represents the UV–Vis spectroscopic measurement of (I) Ag_2O micro powders from which silver/silver oxide nanoparticles were produced after 72 h completion of reaction with fungus *Fusarium oxysporum* and (II) biotransformed Ag/Ag_2O NPs. Color changes during the reaction were the initial visual conformation for the formation of nanoparticles. The spectrum shows two absorption maxima at 265 nm and 415 nm for biotransformed Ag/Ag_2O NPs whereas no peak was observed for Ag_2O micro powder. The SPR (surface plasmon resonance)) absorption at 415 nm specified the presence of Ag nanoparticles with Ag_2O nanoparticles (Ravichandran et al. 2016; Elemike et al. 2017). The absorption peak at 265 nm corresponds to fungus secreted aromatic amino acid which worked as capping molecules (Khan and Ahmad 2013). Being the nanoparticles capped by organic molecules, it showed non-flocculating and water-dispersible in nature. The missing absorption edge for Ag_2O micro-powder is due to the absence of SPR of micron size silver oxide particles.

Fourier transform infrared spectroscopy (FT-IR) was performed to ensure the presence of a characteristic Ag–O stretching band and the bond vibration frequency for capping stabilized protein biomolecules. FT-IR spectrum of biotransformed silver oxide nanoparticles (Fig. 1b) showed an absorption peak at 570 cm^{-1} correspond to the Ag–O vibration (Ravichandran et al. 2016). The strong absorptions at 3400 cm^{-1} and 2937 cm^{-1} were assigned for O–H (alcohol) or N–H (amines) stretching vibration and C–H (alkyl) stretching. The peak at 1629 cm^{-1} attribute to N–C = O amide I bond which is the most intense absorption band in proteins whereas the band at 1580 cm^{-1} is a representative of amide II mainly come from in-plane N–H bending. The peaks entered at 1398 cm^{-1}, 1025 cm^{-1} and 661 cm^{-1} can be associated with C–N stretching of amine, alcohol/phenolic stretching, and aromatic C–H bending (Manikandan et al. 2017).

The size of nanoparticles are confirmed by Transmission electron microscopy (TEM). The micron size of parent silver oxides is shown in Fig. 2a whereas the formation and spherical shape of biotransformed silver/silver oxide nanoparticles are represented by the TEM images shown in Fig. 2b and c respectively. The particle size distribution histogram (Fig. 2d) obtained from TEM analysis shows the mean particle size is 6.43 nm including standard error of 0.05 nm. To investigate inter planer distance and crystallinity HR-TEM (Fig. 2e) and Selected area electron diffraction (SAED) (Fig. 2f) has been carried out respectively. Both of these analyses illustrate that the Ag/Ag_2O NPs are crystalline and confirmed the presence of (111) plane which is further confirmed by XRD.

The XRD diffraction pattern of biosynthesized Ag_2O nanoparticles (Fig. 3b) shows four distinct peaks at 27.4, 32.1, 37.2 and 64.5 corresponding to the diffraction plane of (110), (111), (200) and (311), confirming the presence of Ag_2O nanoparticle same as reported data of Ag_2O (Taufik and Saleh 2018). Additionally, several reflection peaks were observed at 37.2, 44.6, 46.2, and 76.3 which indexed to (111), (200), (211), and (311) plans of FCC silver respectively (Jalees et al. 2018). The XRD diffraction

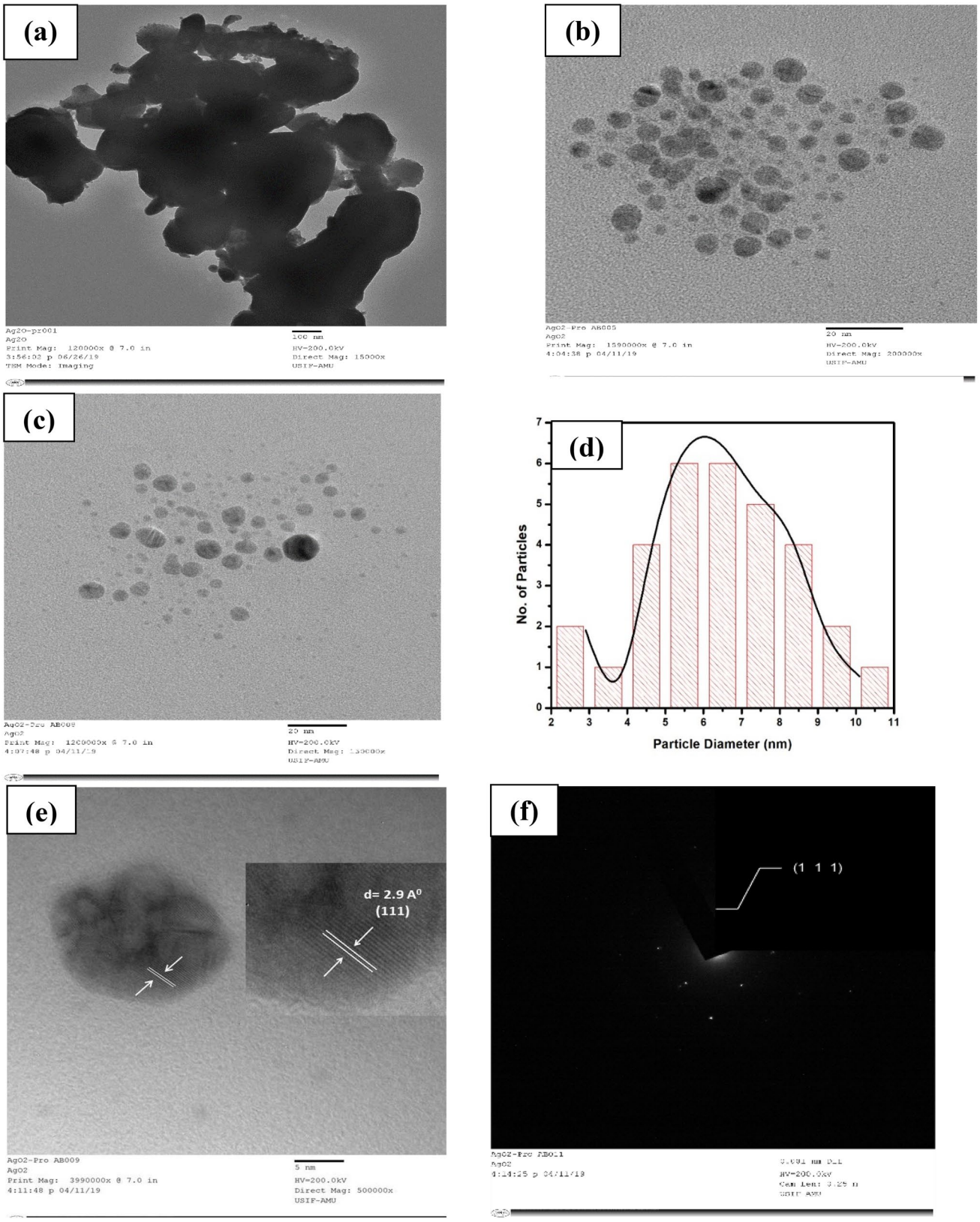

Fig. 2 **a** TEM image of parent Ag_2O micropowder. **b**, **c** TEM image of biotransformed Ag/Ag_2O nanoparticles. **d** Particle size distribution of biotransformed Ag/Ag_2O nanoparticles obtained from TEM image. **e** HR-TEM images of biotransformed Ag/Ag_2O nanoparticles showing inter-planer distance (d-spacing). **f** SAED pattern of biotransformed Ag/Ag_2O nanoparticles

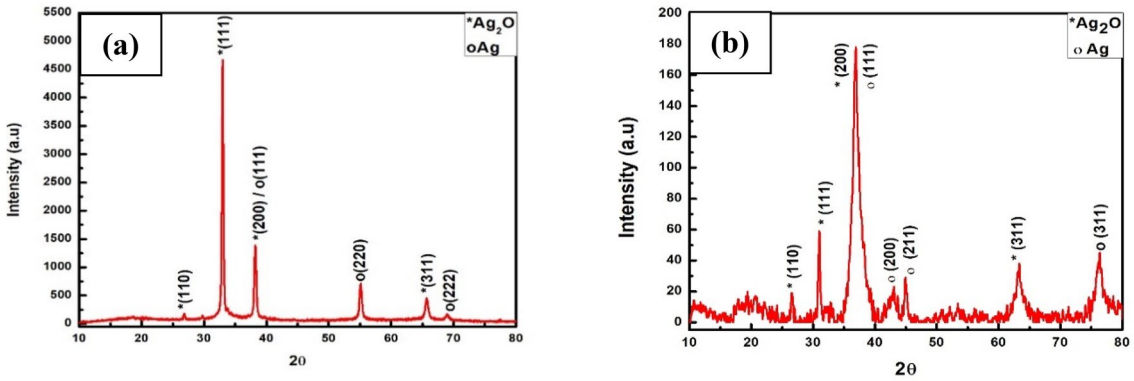

Fig. 3 **a** X-ray diffraction patterns of Ag_2O micropowder. **b** X-ray diffraction patterns of biosynthesized Ag/Ag_2O Nanoparticles

pattern also demonstrates that the most intense diffraction peak observed at 37.2 also confirmed the presence of Ag nanoparticles with Ag_2O nanoparticles and the peak indexed as plane (111) for Ag and plane (200) for Ag_2O. The XRD pattern was also used for the estimation of the mean grain size of mycogenic Ag/Ag_2O NPs by calculating the breadth of the Bragg's reflections using Debye–Scherer's formula and it was found to be 9.95 nm. It also observed that the computed mean size of silver oxide nanoparticles by XRD and the average size calculated from the TEM image by plotting the Histogram is approximately the same. The width of the XRD diffraction peak for biotransformed Ag/Ag_2O nanoparticles is much greater than the diffraction peak width of Ag_2O micro powder (Fig. 3a) which also confirmed the biotransformation of Ag_2O micro powder into Ag/Ag_2O NPs.

A typical cyclic voltammogram recorded at 25 °C is shown in Fig. 5a and Fig. 4a for silver oxide microparticles and silver/silver oxide nanoparticles (black line) respectively. Both voltammograms show three oxidation peaks (A1, A2 and A3) in the anodic sweep. However, three reduction peaks (C1, C2 and C3) were observed for micron Ag_2O while four reduction peaks were marked for mycogenic Ag/Ag_2O nanoparticles (C1, C2, C3 and C4) in the cathodic sweep. Comparison with literature data (Riyantoa and Rizki 2020) we can assign the anodic peaks at A1, A2 and A3 for the formation of AgO^- or AgOH, Ag_2O and AgO whereas cathodic peaks at C1, C2 and C3 are leveled for the reduction of AgOH, Ag_2O and AgO. It is believed that the following redox reactions are responsible for the appeared peaks.

$$Ag + OH^- \leftrightarrow AgOH + e^- \text{ (A1/C1)}$$

$$2Ag + 2OH^- \leftrightarrow Ag_2O + H_2O + 2e^- \text{ (A2/C2)}$$

$$Ag_2O + 2OH^- \leftrightarrow 2AgO + H_2O + 2e^- \text{ (A3/C3)}$$

The appeared cathodic current peak at C4 is ascribable to the subsequent re-dissolution of AgO (most well-known as mixed oxide $Ag^{I}Ag^{III}O_2$) (Hernández-Ramírez et al. 2009).

$$2AgO\left(Ag_2O_2\right) + 2e^- \rightarrow 2AgO^-(C4)$$

This reduction peak indicates the improved electrochemical activity of nano Ag/Ag_2O (Habekost 2016). There are no characteristic peaks observed when we used uncoated glassy carbon electrode during the forward and backward scan (red line).

Figures 5b and 4b represent comparative cyclic voltammograms that were recorded at different glucose concentrations where micron Ag_2O particles and mycogenic Ag/Ag_2O nanoparticles were used as a working electrode. The peaks represented by (I) and (II) corresponding to cycle1 and cycle2 recorded in the absence of glucose indicate stable current conditions. The anodic current peak A3 decreases with an increase in glucose concentration. The decrease in anodic current peak A3 in the presence of glucose can be interpreted as oxidation of glucose into gluconic acid by the reduction of Ag_2O. As long as Ag_2O participates in glucose oxidation, its concentration decreases with increasing the concentration of glucose and hence the anodic current peak A3 decreases. Figure 4c represents the possible mechanism of electrochemical glucose sensing. The linear plot of A3 peak current vs glucose concentration ($R^2 = 0.995$) corresponds to mycogenic Ag/Ag_2O nanoparticles (Fig. 4d) suggested that the capping protein and oxidized gluconic acid does not interfere with glucose oxidation reaction while there was no such linear response (Fig. 5c) observed in case of micron Ag_2O particles (Fig. 5b) due the interaction of oxidized gluconic acid with Ag (A1 current peak decreases, Fig. 5a) to form silver gluconate.

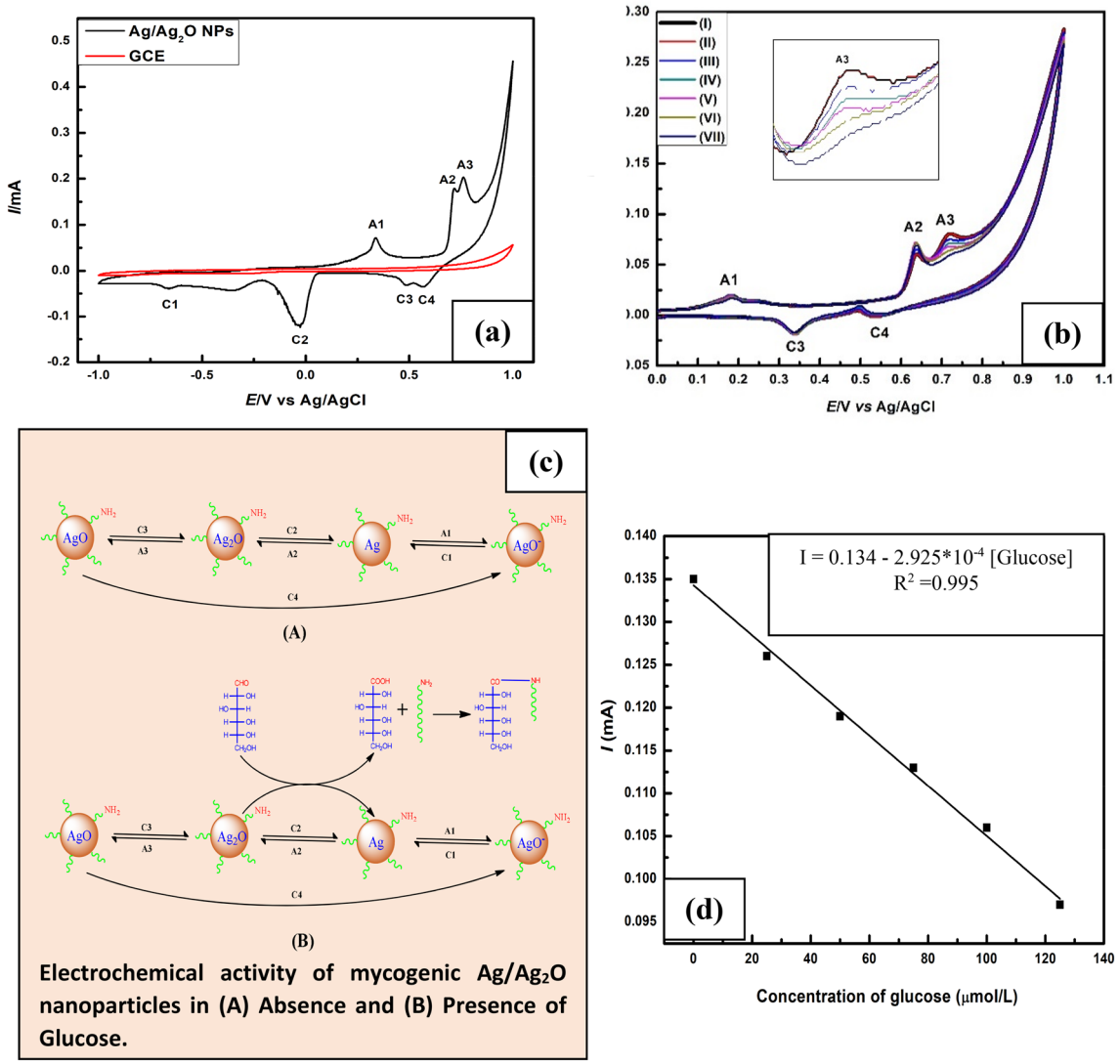

Electrochemical activity of mycogenic Ag/Ag_2O nanoparticles in (A) Absence and (B) Presence of Glucose.

Fig. 4 Cyclic Voltammograms of **a** Ag/Ag_2O Nanoparticles deposited on Glassy carbon electrode (GCE) in alkaline electrolyte. **b** Cyclic Voltammograms of mycogenic Ag/Ag_2O nanoparticles in absence of glucose [cycle1 (I) and cycle2 (II) and in the presence of glucose having concentration 25 µmol/L (III), 50 µmol/L (IV), 75 µmol/L (V), 100 µmol/L (VI), 125 µmol/L (VII). **c** Possible mechanism for non-enzymatic glucose sensing. **d** Plot of A3 peak current vs. glucose concentration

The degradation of MB with $NaBH_4$ was monitored in the presence and absence of mycogenic Ag/Ag_2O NPs through UV–Vis spectrophotometer. The gradual decrease in UV–Vis absorption peak at wavelength 664 nm in the presence of Ag/Ag_2O NPs (Fig. 6a) with reaction time confirmed its catalytic ability for MB dye degradation as there was no degradation observed in absence of Ag/Ag_2O NPs (Fig. 6b). The catalytic efficiency of Ag/Ag_2O NPs has been evaluated by examining the absorption spectra recorded at various concentrations of Ag/Ag_2O NPs i.e., 0.1 (A), 0.2 (B), 0.3 (C), 0.4 (D) and 0.5 mg/ml (E) and compared with the degradation ability of control Ag_2O microparticles (0.5 mg/ml) (Fig. 6c). The percentage (%) degradation bar graph (Fig. 6d) at the indicated higher concentration (0.5 mg/ml) for control Ag_2O microparticles (50.6%) and mycosynthesized Ag/Ag_2O NPs (86.5%) shows enhanced catalytic activity of NPs by 36% at a fixed time of 10 min. The enhanced catalytic activity was attributed as Ag/Ag_2O NPs provide more surface area as compared with the bulk Ag_2O microparticles for catalytic degradation reaction.

To study the thermal stability, thermogravimetric analysis was performed to measure the mass change of biosynthesized Ag/Ag_2O NPs as a function of temperature at a heating rate of 10 ℃/min under nitrogen atmosphere. TGA

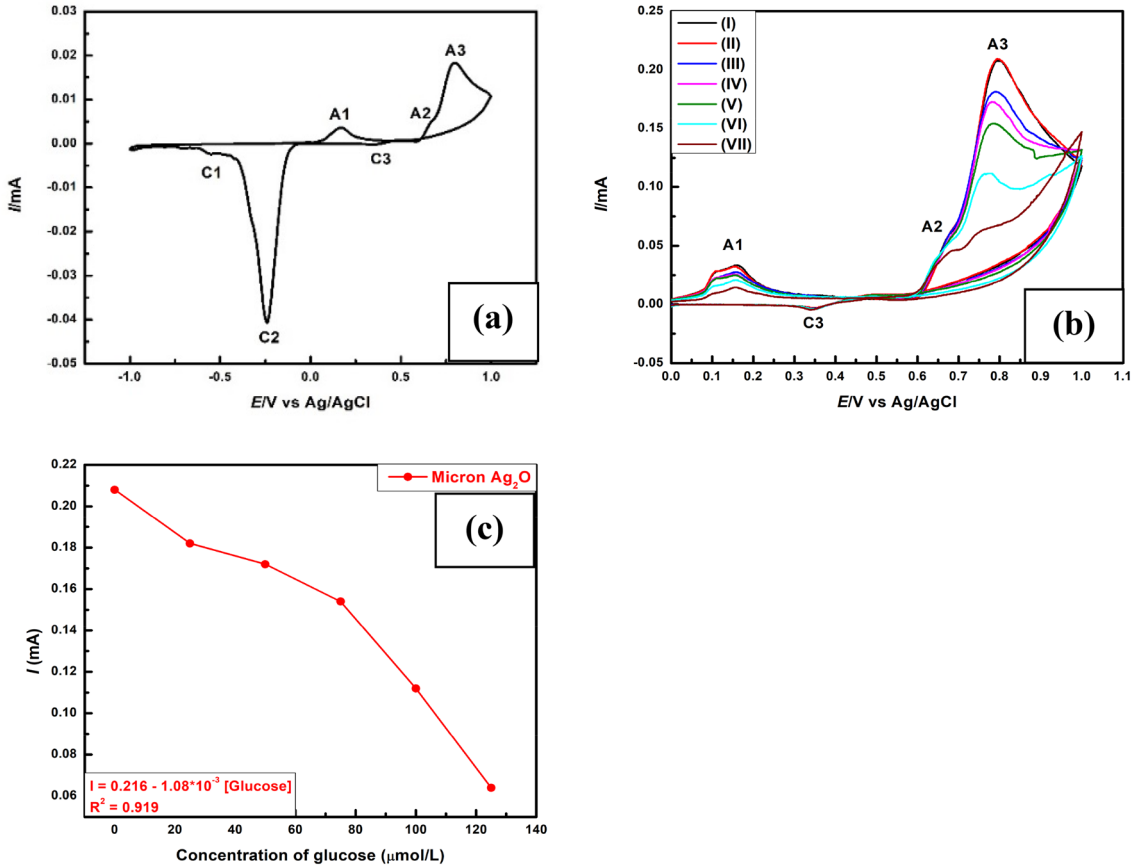

Fig. 5 **a** Cyclic Voltammograms of micron Ag_2O particles deposited on Glassy carbon electrode (GCE) in alkaline electrolyte. **b** Cyclic Voltammograms of micron Ag_2O particles in absence of glucose [cycle1 (I) and cycle2 (II)] and in the presence of glucose having concentration 25 µmol/L (III), 50 µmol/L (IV), 75 µmol/L (V), 100 µmol/L (VI), 125 µmol/L (VII). **c** Plot of A3 peak current vs. glucose concentration

measurement of Ag/Ag_2O NPs (Fig. 7a) shows a continuous weight loss with three sharp changes starting at 100 °C, 230 °C, and 365 °C. The effective weight loss starting at 100 °C means the loss of moisture whereas weight loss started at 230 °C results from the degradation of protein molecules which indicates that the silver oxide nanoparticles are surrounded by capping protein. The thermal degradation starting at 365 °C attributed to the transformation of Ag_2O into Ag nanoparticles (Taufik and Saleh 2018; Siddiqui et al. 2013).

$$Ag_2O \rightarrow 2Ag + \tfrac{1}{2}\, O_2$$

Differential scanning calorimetry (DSC) analysis was performed as a complementary technique of TGA with a heating rate 10 °C/min. The scanning was carried out from 200 °C to 400 °C for measurement of the enthalpy change. DSC profile of biotransformed silver/silver oxide nanoparticles shows two peaks (Fig. 7b) at 230 °C and 365 °C which is good agreement with the TGA measurement. The DSC curve shows an endothermic peak for degradation of protein molecules whereas the transformation of Ag_2O nanoparticles into Ag nanoparticles followed the exothermic process. Differential scanning calorimetry (DSC) analysis was also displayed the required temperature for the thermal decomposition of silver oxide nanoparticles to silver nanoparticles (365 °C) is lower than the temperature required for the decomposition of silver oxide micropowder to silver oxide nanoparticles (400 °C) (Shin et al. 2013).

Figures 8 and 9 represent the antifungal and antibacterial activity of mycogenic silver oxide nanoparticles against *Aspergillus niger* and *Bacillus subtilis* respectively. The clearance zone observed in b and c clearly stabilised the antimicrobial activity of these biogenic Ag/Ag_2O NPs.

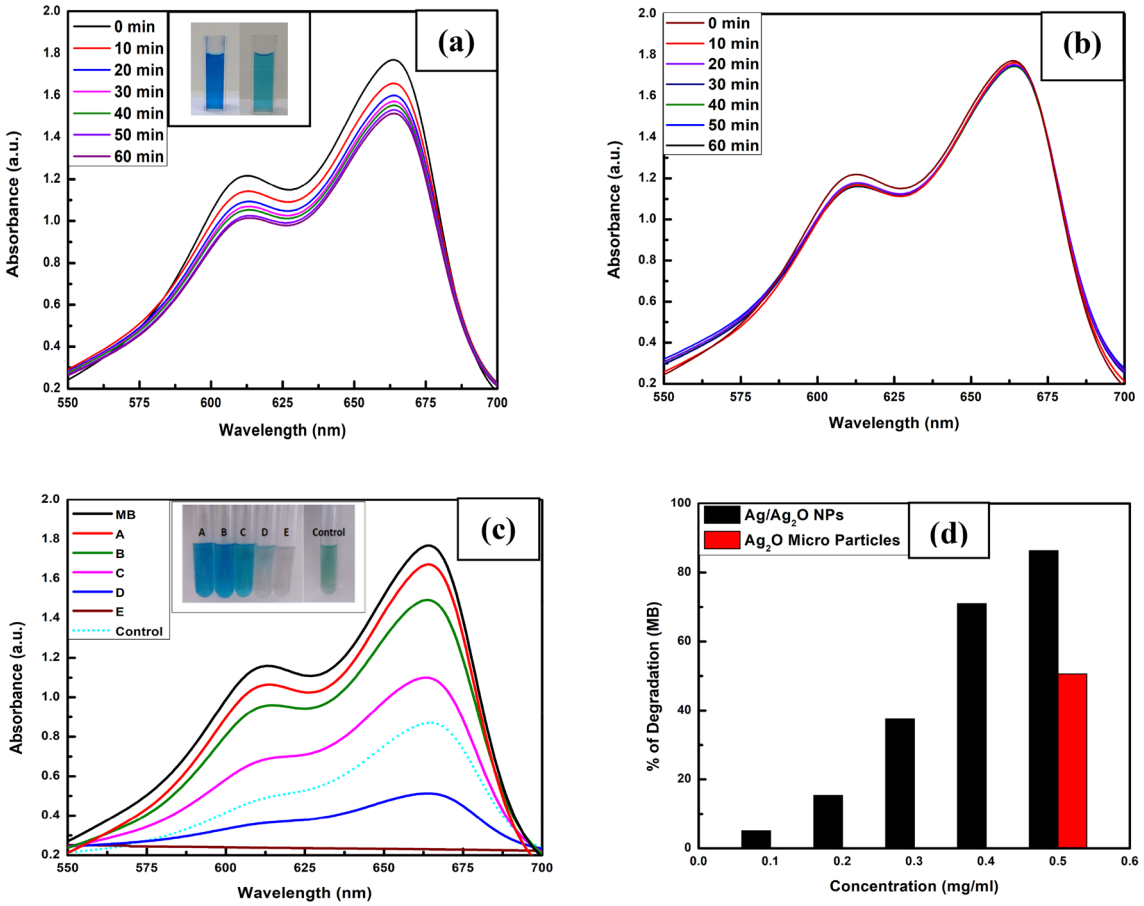

Fig. 6 UV–Vis absorption spectra of the aliquots recorded with 0.1 mg/ml Ag/Ag_2O NPs (**a**) and Without (**b**) Ag/Ag_2O NPs at a regular time interval of 10 min ambient temperature. **c** Ag/Ag_2O NPs weight dependent (from 0.1 mg/ml to 0.5 mg/ml) absorption spectra at a fixed time of 10 min and **d** Percentages (%) of MB degradation graph

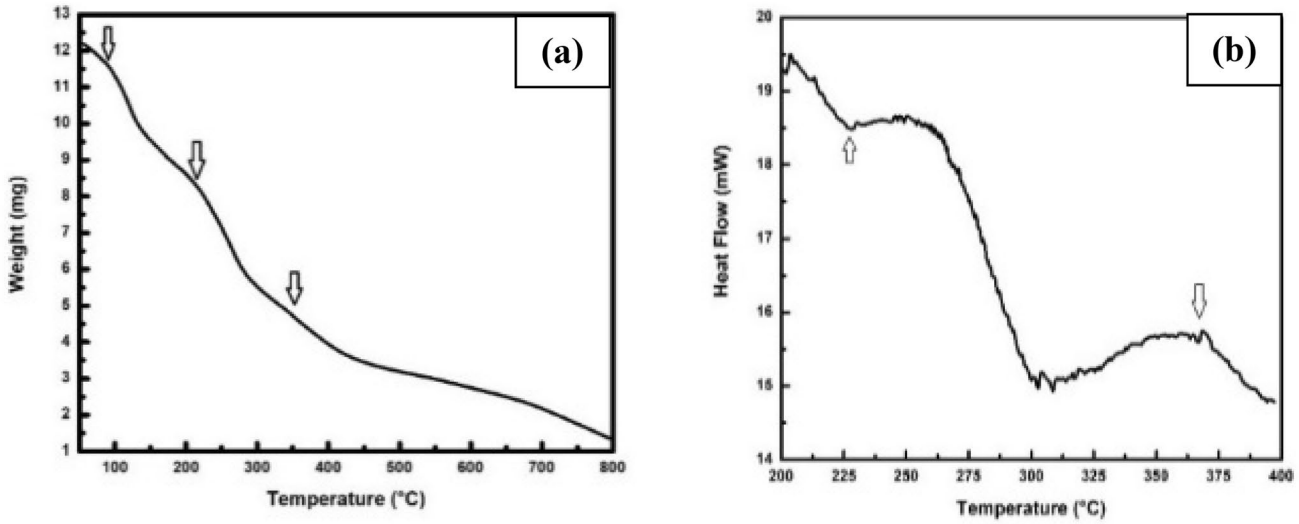

Fig. 7 **a** TGA curve of biosynthesized Ag/Ag_2O nanoparticles. **b** DSC curve of biotransformed Ag/Ag_2O nanoparticles

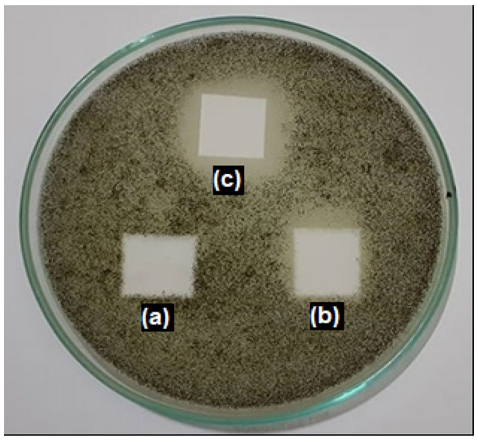

Fig. 8 Antifungal activity of mycogenic (biotransformed) Ag/Ag_2O nanoparticles showing control with distilled water (**a**) and mycogenic Ag/Ag_2O nanoparticles (**b**, **c**)

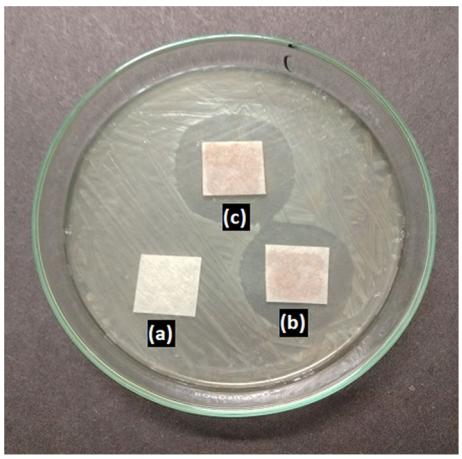

Fig. 9 Antibacterial activity of mycogenic (biotransformed) Ag/Ag_2O nanoparticles showing control with distilled water (**a**) and mycogenic Ag/Ag_2O nanoparticles (**b**, **c**)

Conclusion

We herein report a highly simple, nontoxic top-down green approach for the production of protein capped, water dispersible, stable Ag/Ag_2O NPs which can be produced in abundance using endophytic fungus *Fusarium oxysporum*. The obtained particle size of synthesized nanoparticles is in the range between 5–10 nm which are crucial for biomedical applications. The electrochemical study of mycogenic Ag/Ag_2O NPs in the presence of glucose shows that it may become a potential candidate for enzyme-free glucose determination and may provide a simple and direct methodology for low-limit detection. These thermally stable green synthesized Ag/Ag_2O NPs exhibited catalytic potency for the degradation of MB dye in presence of reducing agent $NaBH_4$. We have also investigated the antimicrobial activity of synthesized Ag/Ag_2O NPs and we found it is an excellent antimicobial agent against *Aspergillus niger* and *Bacillus subtilis.* At a time when drug resistance is increasing at an alarming rates, our mycogenic Ag/Ag_2O NPs exhibiting antimicobial activity will find major use in the development of a newer improved drug.

We believe that this novel top-down approach of using endophytic fungus *Fusarium oxysporum* to reduce the size of desired material into water-dispersible nanomaterials, can be extended to many other bulk material and nanoparticle synthesis in large amounts, as compare to any other biological or chemical or physical methods. These electrochemically stable nanoparticles can be used in electrochemical sensing, catalysis, advanced materials, antimicrobials and in many biomedical applications. Thus we can say our Ag/Ag_2O NPs are multifunctional in nature.

Acknowledgements We acknowledge the Department of Biotechnology (DBT), Government of India, for setting up a Centre of Excellence (COE, BT/PR1-3584/COE/34/29/2015) at Interdisciplinary Nanotechnology Centre (INC), Aligarh Muslim University, AMU, Aligarh, UP-202002, India. We thank Mr. Ashraf Ali Khan and Mr. Alim Kazmi of INC for their technical assistance.

Declarations

Conflict of interest The authors have no conflicts of interest in the publication.

References

Ahmad A, Jagdale T, Dhas V, Khan S, Patil S, Pasricha R, Ravi V, Satishchandra O (2007) Fungus based synthesis of chemically difficult to synthesize multifuncational nanoparticles of $CuAlO_2$. Adv Mater 19:3295–3299

Bansal V, Ahmad A, Sastry M (2006) Fungus mediated biotransformation of amorphous silica in rice husk to nanocrystalline silica. J Am Chem Soc 128:14059–14066

Chen LF, Xie HQ, Li J (2012) Electrochemical glucose biosensor based on silver nanoparticles/multiwalled carbon nanotubes modified electrode. J Solid State Electrochem 16:3323–3329

Derikvand F, Bigi F, Maggi R, Piscopo CG, Sartori G (2010) Oxidation of hydroquinones to benzoquinones with hydrogen peroxide using catalytic amount of silver oxide under batch and continuous-flow conditions. J Catal 271:99–103

Dhoondia ZH, Chakraborty H (2012) Lactobacillus mediated synthesis of silver oxide nanoparticles. Nanomater Nanotechnol 2(15):2012

Edison TNJI, Atchudan R, Kamal C, Lee YR (2016) Caulerpa racemosa: a marine green alga for eco-friendly synthesis of silver nanoparticles and its catalytic degradation of methylene blue. Bioprocess Biosyst Eng 39:1401–1408

Elemike EE, Onwudiwe DC, Ekennia AC, Sonde CU, Ehiri RC (2017) Green synthesis of Ag/Ag_2O nanoparticles using aqueous leaf extract of eupatorium odoratum and its antimicrobial and mosquito larvicidal activities. Molecules 22:674

Fuglerud SS, Milenko KB, Ellingsen R, Aksnes A, Hjelme DR (2019) Glucose sensing by absorption spectroscopy using lensed optical fibers. Appl Opt 58(10):2456–2462

Habekost A (2016) Experimental investigations of alkaline silver-zinc and copper-zinc batteries. World J Chem Educ 4(1):4–12

Hernández-Ramírez VA, Alatorre-Ordaz A, Yepez-Murrieta ML, Ibanez JG, Ponce-de-León C, Walsh FC (2009) Oxidation of the borohydride ion at silver nanoparticles on a glassy carbon electrode using pulsed potential techniques. Adv Solid State Electrochem Sci Technol 2(1):211–225

Ibarra HO, Vitela RT, Salazar SG, Casillas N, de León CP, Frank C (2018) Walsh enhancement of antibacterial efficiency at silver electrodeposited on coconut shell activated carbon by modulating pulse frequency. J Solid State Electrochem 22:749–759

Ida Y, Watase S, Shinagawa T, Watanabe M, Chigane M, Inaba M, Tasaka A, Zaki MI (2008) Direct electrodeposition of 1.46 eV bandgap silver (I) oxide semiconductor films by electrogenerated acid. Chem Mater 20:1254

Islam SKN, Naqvi SMA, Ahmad A, Parveen S (2021) Endophytic fungus-assisted biosynthesis, characterization and solar photocatalytic activity evaluation of nitrogen-doped Co_3O_4 nanoparticles. Appl Nanosci 11:1651–1659

Jalees M, Lawrence RS, Chhattree A, Yadav M, Sailus N (2018) Green synthesis of silver oxide nanoparticles prepared from waste part of mango peels. Int J Pure App Biosci 6(3):502–508

Khan S, Ahmad A (2014) Enzyme mediated synthesis of water dispersible, naturally protein capped, monodispersed gold nanoparticles; characterization and mechanistic aspects. RSC Adv 4:7729–7734

Khan SA, Ahmad A (2013) Phase, size and shape transformation by fungal biotransformation of bulk TiO_2. Chem Eng J 230:367–371

Khan NT, Khan MJ, Jameel J, Jameel N, Rheman SUA (2017) An overview: biological organisms that serves as nanofactories for metallic nanoparticles synthesis and fungi being the most appropriate. Bioceram Dev Appl 7:101. https://doi.org/10.4172/2090-5025.1000101

Lee H, Hong YJ, Baik S, Hyeon T, Kim DH (2018) Enzyme-based glucose sensor: from invasive to wearable device. Adv Healthcare Mater 7:1701150

Manikandan V, Velmurugan P, Park J-H, Chang W-S, Park U-J, Jayanthi P, Cho M, Oh B-T (2017) Green synthesis of silver oxide nanoparticles and its antibacterial activity against dental pathogens. 3 Biotech 7(1):72

Maurício A, Papi P, Caetano FR, Bergamini MF, Marcolino-Junior LH (2017) Facile synthesis of a silver nanoparticles/polypyrrole nanocomposite for nonenzymatic glucose determination. Mater Sci Eng C 75:88–94

Petrov VV, Nazarova TN, Korolev AN, Kopilova NF (2008) Thin sol–gel SiO2–SnOx–AgOy films for low temperature ammonia gas sensor. Sens Actuators B Chem 133:291–295

Pishbin MH, Mohammadi AR, Nasri M (2007) Optimisation of manufacturing parameters for an Ni–Ag fuel cell electrode. Fuel Cells 7(4):291–297. https://doi.org/10.1002/fuce.200600027

Ravichandran S, Paluri V, Kumar G, Loganathan K, Venkata BRK (2016) A novel approach for the biosynthesis of silver oxide nanoparticles using aqueous leaf extract of Callistemon lanceolatus (Myrtaceae) and their therapeutic potential. J Exp Nanosci 11(6):445–458

Riyantoa, Rizki AT (2020) Cyclic voltammetry of glucose, uric acid, and cholesterol using gold electrode. AIP Conf Proc 2229(1): 030037. https://doi.org/10.1063/5.0002791

Saha J, Begum A, Mukherjee A, Kumar S (2017) A novel green synthesis of silver nanoparticles and their catalytic action in reduction of Methylene Blue dye. Sustain Environ Res 27:245–250

Shabbir SA, Tariq S, Ashiq MGB, Khan WA (2019) Non-enzymatic glucose sensor with electrodeposited silver/carbon nanotubes composite electrode. Biosci Rep 39:20181983

Shahriary L, Athawale AA (2015) Electrochemical deposition of silver/silver oxide on reduced graphene oxide for glucose sensing. J Solid State Electrochem 19:2255–2263

Shankar SS, Rai A, Ankamwar B, Singh A, Ahmad A, Sastry M (2004) Biological synthesis of triangular gold nanoprisms. Nat Mater 39:482–488

Sharma VK, Yngard RA, Lin Y (2009) Silver nanoparticles: green synthesis and their antimicrobial activities. Adv Coll Interface Sci 145:83–96

Shin D-Y, Yi G-R, Lee D, Park J, Lee Y-B, Hwang I, Chun S (2013) Rapid two-step metallization through physicochemical conversion of Ag_2O for printed "black" transparent conductive films. Nanoscale 5(11):5043–5052

Siddiqui MRH, Adil SF, Assal ME, Ali R, Al-Warthan A (2013) Synthesis and characterization of silver oxide and silver chloride nanoparticles with high thermal stability. Asian J Chem 2(6):3405–3409

Tarahovsky YS, Kim YA, Ivanitsky GR (2008) Taxifolin fibers as biomedical nanomaterial. Dokl Biochem Biophys 422:265

Taufik A, Saleh R (2018) The influence of graphene on silver oxide synthesis through microwave assisted method. AIP Conf Proc 2023(1):020018. https://doi.org/10.1063/1.5064015

Wang W, Zhao Q, Dong J, Li J (2011) A novel silver oxides oxygen evolving catalyst for water splitting. Int J Hydrogen Energy 36:7374–7380

Wei W, Mao X, Luis AO, Donald RS (2011) Oriented silver oxide nanostructures synthesized through a template-free electrochemical route. J Mater Chem 21:432–438

Yong NL, Ahmad A, Mohammad AW (2013) Synthesis and characterization of silver oxide nanoparticles by a novel method. Int J Sci Eng Res 4(5):155–158

Zhu H, Li L, Zhou W, Shao Z, Chen X (2016) Advances in non-enzymatic glucose sensors based on metal oxides. J Mater Chem B 4:7333